



1 **Precipitation rather than wind drives the response of East Asian** 2 **forests to tropical cyclones**

3 Yi-Ying Chen¹ and Sebastiaan Luyssaert²

4 ¹Research Center for Environmental Changes, Academia Sinica, Taipei, 11529, Taiwan

5 ²Faculty of Science, Vrije Universiteit Amsterdam, Amsterdam, 1081, The Netherlands

6 *Correspondence to:* Yi-Ying Chen (yiyingchen@gate.sinica.edu.tw)

7 **Abstract.** Forests disturbance by tropical cyclones is documented by field studies of exceptionally strong cyclones
8 and satellite-based approaches attributing decreases in leaf area. The biases that come with such approaches may limit
9 our understanding of the impact of cyclones in general. This study overcomes such biases by starting the analysis from
10 the observed storm tracks rather than the observed damage. Changes in forest leaf area in East Asia were assessed by
11 jointly analyzing the cyclone tracks, climate reanalysis, and changes in satellite-based leaf area following the passage
12 of 145 ± 42 cyclones. Sixty days following their passage, $14 \pm 6\%$ of the cyclones resulted in a decrease and $55 \pm 21\%$
13 showed no change in leaf area compared to nearby forest outside the storm track. For a surprising $31 \pm 6\%$ of the
14 cyclones, an increase in leaf area was observed. Further analysis revealed that cyclones bringing abundant precipitation
15 to dry forest soils in summer could relieve water stress within the storm track increasing its leaf area compared to
16 vegetation outside the storm track. This observation calls for refining the present-day view of cyclones as agents of
17 destruction toward a more nuanced vision that recognizes that cyclones could have minor or even positive effects on
18 leaf area and as such on forest growth.

19 **Main Text**

20 Each year almost 30 cyclones, about one-third of the world's tropical cyclones, develop over the Pacific Ocean north
21 of the equator (Landsea, 2000) where a subtropical ridge steers them mainly west and northwest towards Eastern Asia,
22 where 90 % make landfall. The majority of the tropical cyclones in the northwestern Pacific basin develop between
23 June and November (Bushnell et al., 2018) and more than half acquire typhoon strength (WMO, 2017). The four most
24 powerful typhoons in the region since 1999, i.e., Morakot in 2009, Megi in 2010, Haiyan in 2013, and another typhoon
25 also named Megi in 2016, claimed over 7,000 lives, left 1,700 missing, and destroyed over 10 billion USD worth of
26 infrastructure and crops according to compilations of mostly local news sources (Yang et al., 2014; Bowen, 2016; Lu
27 et al., 2017; OCHA, 2010). Although natural ecosystems, such as forests, have adapted to recurring high wind speeds
28 (Eloy et al., 2017; Louf et al., 2018; Curran et al., 2008), stem breakage is almost unavoidable at wind speeds above
29 40 m s^{-1} (Virost et al., 2016) but has been widely reported at wind speeds well below this threshold together with other
30 damage (Tang et al., 2003; Chiu et al., 2018; Chang et al., 2020a). Despite the economic importance of forests in the
31 region (Barbier, 1993; Vickers et al., 2010), an overall assessment of the damage of tropical cyclones on forest
32 resources is still lacking.



33

34 By jointly analyzing cyclone tracks (JTWC, 2019), climate reanalysis data (ECMWF, 2019), and satellite-based
35 proxies of soil dryness (Beguería et al., 2014), land cover (ESA, 2017), and leaf area (Martins et al., 2020), we
36 estimated: (a) the potential forest area damaged by tropical cyclones, (b) the impact of tropical cyclones on leaf area,
37 and (c) the main drivers of this impact. Previous studies attributed decreases in leaf area or related satellite-based
38 indices to different disturbance agents including cyclones (Ozdogan et al., 2014; Takao et al., 2014; Honkavaara et
39 al., 2013; Forzieri et al., 2020). A damage-based approach is designed to identify only decreases in leaf area, thus
40 failing to identify events in which tropical cyclones left the leaf area unaltered or increased it. In contrast, this study
41 starts the analysis from the actual storm tracks which allows for an unbiased assessment of the impact of cyclones on
42 forests (Blanc and Strobl, 2016).

43

44 The land area affected was identified for each of the 580 tropical cyclones that occurred in the study region between
45 1999 and 2018, considering that cyclone-driven damage could only occur within the storm track at locations that
46 experienced high wind speeds and/or high precipitation. Pixels within the storm track for which the threshold values
47 were exceeded were classified as affected areas, the remaining pixels served as a cyclone-specific reference area. The
48 uncertainty derived from defining the width of the storm track (Willoughby and Rahn, 2004) and determining which
49 wind speeds and amounts of precipitation could result in damage are accounted for by an ensemble of nine related
50 definitions with different threshold values (**Table A1**). Uncertainties reported in this study represent the standard
51 deviation across the nine definitions for the affected area.

52

53 Since 1999, 224 ± 69 Mha of forest in the study region experienced conditions that may have resulted in cyclone-
54 driven damage, at least once every decade (**Fig. 1A**). At decadal or longer return intervals, a single cyclone may greatly
55 affect ecosystem functioning, forest structure and species composition of the forest (Xi, 2015; Castañeda-Moya et al.,
56 2020). No less than 54 ± 26 Mha, including 70 % of the tropical forest in the region, experienced potentially damaging
57 conditions at least once per year, and are thus classified as being under chronic wind stress (**Fig. 1A**). Lower estimates
58 from the rain-only definitions closely matched the 70 Mha yr^{-1} that was reported following a similar approach in which
59 the affected area was defined as a 100 km buffer zone along the storm track (Lin et al., 2020).

60

61 Irrespective of the definition of the affected area, the coefficient of variation of the between-year variation in
62 potentially damaged areas ranged from 15 to 20 % (**Fig. 1B**). Excluding the four most powerful typhoons that occurred
63 in the region since 1999 changed the average coefficient of variation from 17 to 16 %. This suggests that the most
64 powerful typhoons make only a small contribution to the total annually potentially affected area in the region. A recent
65 literature review reported, however, that 66 % of the research papers in this area have examined the effects of only
66 about 6 % of the most powerful cyclones (Lin et al., 2020). The relatively small contribution of those events to the
67 potentially damage area suggests that in regions with frequent tropical storms, disturbance ecology would benefit from



68 broadening its scope by examining the effects and recovery of a representative sample of tropical cyclones, rather than
69 focusing on the most devastating events.

70

71 The different definitions of affected area (**Table A1**) consistently show a high potential for forest damage over island
72 and coastal regions located between 10- and 35-degrees latitude (**Fig. 1C**). Although damage potential is the outcome
73 of an interplay between cyclone frequency, cyclone intensity and the presence of forests, the high potential in this
74 region is largely driven by the frequency of tropical cyclones (**Fig. A1**), i.e., two or more cyclones making landfall
75 per year. Depending on how the affected area is defined, there is a second region located between 40 and 50 degrees
76 north with a high potential for storm damage (**Fig. 1C**). In this region, the potential damage is the outcome of the high
77 forest cover resulting in a strong dependency on the assumed width of the storm track (**Fig. A1**).

78

79 The impact of a tropical cyclone on leaf area was calculated based on the adjusted Hedge's effect size by comparing
80 the change in leaf area before and after the cyclone in the affected area with the change before and after the cyclone
81 in the reference area for each individual cyclone (**Eq. 1**). Using a reference area that is specific to each cyclone means
82 that seasonal dynamics related to leaf phenology and seasonal monsoons can be accounted for in the effect size, which
83 is a unitless description of the mean change in leaf area normalized by its standard deviation (**Eq. 1**). A positive or
84 negative effect size respectively denotes an increase or decrease in leaf area following the passage of a tropical cyclone.

85

86 A total of 316 ± 22 tropical cyclones or $54 \pm 4\%$ of the storm events under study could not be further analysed (**Table**
87 **A1**) because leaf area index (LAI) observations were missing from either the affected area, the reference area, or both,
88 thus violating the requirements for calculating the effect size (**Eq. 1**). Of the remaining 264 ± 22 tropical cyclones,
89 only 145 ± 42 passed the additional quality checks necessary to be retained for further analysis in this study: (i) have
90 a less than $0.5 \text{ m}^2 \text{ m}^{-2}$ difference in the leaf area between the reference and affected area prior to the passage of the
91 storm signifying that prior to the storm the reference area is indeed similar to what will become the affected area; and
92 (ii) have an effect size that is larger than the noise of the remotely sensed leaf area. Despite the loss of around 75 %
93 of the events, the quality control criteria resulted in an unbiased sample in terms of wind speed (**Fig. A2**).

94

95 The effect size of 79 ± 31 events was less than the noise of the remotely sensed change in leaf area suggesting that for
96 $55 \pm 21\%$ of the cyclones, the change in leaf area 60 days after a cyclone passed was too small to distinguish it from
97 the noise of present-day remote sensing technology. Nevertheless, ecological theory predicts forest dwarfing in regions
98 with high cyclone frequencies directly through gradual removal of taller trees over many generations (Lin et al., 2020;
99 McDowell et al., 2020) and indirectly through the loss of nutrients (Tang et al., 2003; Lin et al., 2011). Where forest
100 dwarfing has occurred, it might be hard to observe the short-term effects of an individual tropical cyclone on forest
101 structure and function (Mabry et al., 1998). Following the terminology of this study, a neutral effect size over regions
102 with high return frequencies would be consistent with structural adaptation to frequent cyclones. Indeed, for regions
103 that experience over 4.5 cyclones per year, the mean effect size was almost zero (**Fig. A3**).



104

105 Tropical cyclones have been widely observed to defoliate and disturb forests because of limb breaking, uprooting,
106 stem breakage and landslides following high wind speeds and heavy precipitation (Wang et al., 2013; Uriarte et al.,
107 2019; Chambers et al., 2007; Douglas, 1999; Lin et al., 2011). Nevertheless, in this study, only 14 ± 6 % of the
108 observed cyclones resulted in a detectable reduction in leaf area as a direct effect of limb breakage, uprooting, stem
109 breakage and landslides, 60 days after their passage. On the other hand, for 31 ± 6 % of the cyclones an increase in
110 leaf area was observed, leading to the question: which conditions lead to an increase (or a reduced decrease) in leaf
111 area between the affected and control areas 60 days following the passage of a tropical cyclone?

112

113 To answer this question, two groups of meta-data were compiled for each of the 145 ± 42 tropical cyclones that passed
114 the quality checks, the first group consisting of five characteristics describing the land surface before the passage of a
115 cyclone and the second group containing five characteristics of the cyclone itself (**Table A2**). Following factorial
116 analysis to identify collinearity between the meta-data in the same group, the explanatory power of the meta-data was
117 quantified as a decrease in the accuracy of a random forest analysis (**Fig. 2**). The random forest analysis was repeated
118 12 times with different combinations of largely uncorrelated meta-data (**Table A3**). Each random forest analysis
119 included the effect sizes and meta-data for all nine definitions of affected area to account for this specific source of
120 uncertainty.

121

122 The statistical analysis showed that accumulation of precipitation during the passage of a cyclone over land makes the
123 largest contribution to the accuracy of the random forest analysis. Randomizing this variable decreased the accuracy
124 of the random forest analysis by 20 to 26 % (**Fig. 2**). Soil dryness quantified as the standardized precipitation and
125 evapotranspiration index (SPEI) at the time of landfall was the second most important variable contributing 2 to 17 %
126 whereas the other meta-data contributed relatively little (-4 to 7 %) to the accuracy of the random forest analysis.
127 Subsequently, the six meta-data with the highest explanatory power were used to build a single regression tree to
128 obtain the environmental drivers and their cut-off values that would best explain the change in leaf area following the
129 passage of a tropical cyclone (**Fig. 3**). In the remainder of this report we focus on the unexpected result, i.e., the
130 increase in leaf area following the passage of a tropical cyclone.

131

132 Cyclones bringing abundant precipitation (≥ 19 mm) during summer months (i.e., after month 6.5) when the forest
133 soil was dry ($\text{SPEI} \leq -0.74$) resulted dominantly (60 to 70 %) in an increase in leaf area along the storm track (**Fig. 3**).
134 The vegetation response was thought to be the outcome of two elements: (a) cyclones making landfall in June, July
135 and August bring 30 to 50 % of the annual precipitation in coastal areas in the study domain (**Fig. A4**) and are thus
136 substantial sources of precipitation. The importance of the precipitation brought by tropical cyclones is confirmed by
137 domain-wide changes in the Standardized Precipitation-Evapotranspiration Index showing that 1070 of the 1309 (82
138 %) cyclones increased soil wetness, and (b) given that much of the study domain has a monsoon climate with relatively
139 little rain in the fall and winter months, the implication is that summer droughts might, for evergreen vegetation, have



140 lasting effects until the next growing season (Chou et al., 2009) unless the drought was ended before the dry season
141 begins. Cyclones, especially those later in summer could bring the precipitation to end summer droughts. For the mid-
142 latitudes, including Korea, China, Taiwan, and Japan, dry summers see an increase in the number of tropical cyclones
143 making landfall which often end the summer drought (Yoo et al., 2015). In South Korea, for example, at least 43 %
144 but possibly as much as 90 % of the summer droughts in coastal regions were abruptly ended by a tropical cyclone
145 (Yoo et al., 2015). Based on our analysis of the Standardized Precipitation-Evapotranspiration Index, 214 of the 1309
146 (16 %) tropical cyclones in East Asia ended a drought.

147

148 An increase in leaf area, following the passage of a tropical cyclone, thus requires three conditions to co-occur: (a) a
149 dry spell, (b) a cyclone making landfall in the region experiencing the dry spell, and (c) the cyclone bringing abundant
150 precipitation to mitigate the soil dryness. Meeting all three conditions at the same time seems unlikely unless there is
151 a physical relationship between summer droughts (a) and tropical cyclones (b). During dry years, a meridional dipole
152 system has been observed in the mid-latitude regions of East Asia with a high pressure system in the region of 40-50
153 N and 150-160E where it is causing the dry spell, and the low pressure system in the region of 20-30N and 120-150N.
154 When such a dipole exists, tropical cyclones generated from the monsoon trough over the West Pacific Ocean are
155 steered through the trough in between the high- and low-pressure systems towards and then along the coast of East
156 Asia (Choi et al., 2010). While travelling along the edges of the high pressure system, the tropical cyclone may disturb
157 the circulation, resulting in an unfavourable environment to sustain the dipole (Choi et al., 2011; Kubota et al., 2016)
158 and bringing precipitation to the dry region that was under the high pressure system.

159

160 By studying a representative sample of tropical cyclones (in terms of storm intensity) (**Fig. A2**), we have shown that
161 over half of the tropical cyclones, i.e., 55 ± 21 %, caused little to no damage to forest leaf area, suggesting that forest
162 dwarfing is a general structural adaption in the study region. Moreover, a third, i.e., 31 ± 6 % of the cyclones in East
163 Asia resulted in an increase in forest growth, because these storms relieved water stress within their track or even
164 ended summer droughts. The observed frequency of positive vegetation responses to cyclones suggests that the present
165 day vision of cyclones as agents of destruction (Altman et al., 2018; Negrón-Juárez et al., 2010; Nelson et al., 1994)
166 should be refined toward a recognition that, depending on the environmental conditions prior to the storm and the
167 characteristics of the storm itself, cyclones could also have limited destructive effects (Lin et al., 2020) or even positive
168 effects on forest growth (Castañeda-Moya et al., 2020; Chang et al., 2020b). As both cyclones (Mei and Xie, 2016)
169 and droughts (Zhao and Dai, 2017) are expected to intensify with global warming, the net direct effect
170 through relieved water stress and indirect effect through possible connections with fire activities (Stuivenvolt Allen et
171 al., 2021) remains highly uncertain.

172

173 **Materials and Methods**

174 **Cyclone track and track diameter**



175 Since 1945, tropical cyclones in the Western North Pacific Ocean have been tracked and their intensity recorded by
176 the Joint Typhoon Warning Center (JTWC). The track data shared by the JTWC consist of quality-controlled six-
177 hourly geolocation observations of the center of the storm with the diameter of the storm being a proxy for its intensity
178 (JTWC, 2019). For the period under consideration, from 1999 to 2018, the geolocations and diameters are the output
179 of the Dvorak model (Dvorak, 1984; Dvorak et al., 1990) derived from visible and infrared satellite imagery. Storm
180 diameters are available starting from January 2003. Prior to this date a generic diameter of 100 km (Lin et al., 2020)
181 is used in this study. Linear interpolation of the six-hourly track data resulted in hourly track data to fill in any gaps
182 in the mapping of the cyclone track.

183

184 In this study, we focus on East Asia which, given the absence of natural boundaries, is defined as the land contained
185 within the northwestern Pacific basin that, according to the JTWC stretches from 100 to 150 degrees east and 0 to 60
186 degrees north. The JTWC compiled track and intensity data for 580 tropical cyclones between 1999 and 2018 in the
187 northwestern Pacific basin. A shorter time series (1999 to 2018) than the entire length of time available (1945 to 2018)
188 was analyzed due to the more limited availability of the leaf area index (LAI) data which had to be jointly analyzed
189 with the track and intensity data to quantify the impact of cyclones on natural ecosystems.

190

191 **Area affected by individual cyclones**

192 The land area thought to be affected by a specific cyclone as well as the reference area for each of the 580 cyclones
193 that occurred in the study area between 1999 and 2018 were identified based on nine different but related definitions
194 (**Table A1**). Each definition comprises a combination of at least two out of three criteria, e.g., the diameter of the
195 cyclone, the maximum wind speed at each location during the passage of the cyclone and accumulated precipitation
196 at each location during the passage of the cyclone. Each forested pixel within each individual storm track was classified
197 as either affected area or reference area based on these nine definitions. Differences in the results coming from
198 differences in the definitions were used throughout the analysis to estimate semantic uncertainties. Uncertainties
199 related to the estimated diameter of the cyclone, wind speed and precipitation data were not accounted for in the
200 calculation of the affected and reference areas because they were thought to be smaller than the uncertainty coming
201 from differences in the definitions themselves.

202

203 The underlying assumption behind the definitions is that forests can only be affected by a specific cyclone if they are
204 located along its storm track. The minimum width of each storm track is the diameter of the cyclone as reported by
205 the JTWC. Following the observation that over the ocean, the actual wind speed exceeds the critical wind speed for
206 stem breakage or uprooting (i.e., 17 m s^{-1} ref. Chen et al., 2018) over a distance of at least three times the diameter of
207 the cyclone (Willoughby and Rahn, 2004), the minimum width of a storm track in which cyclone-related forest damage
208 could occur is defined as three times the diameter recorded by the JTWC although wind speeds drop dramatically
209 when cyclones make land fall (Kaplan and Demaria, 2001). The minimum width of a storm track over land should,



210 therefore, be reduced compared to the observations over the ocean. This study used three different widths to define a
211 storm track, i.e., two, three or four times the recorded diameter (**Table A1**).

212

213 Being located within the track of a specific cyclone is essential but not sufficient for damage to occur. Within a storm
214 track, only forested pixels that experienced high wind speeds or high precipitation were counted as in the potentially
215 affected area. Forest pixels that were located within the storm track but did not experience high wind speeds or high
216 precipitation were counted as in the reference area. Note that to better account for the uncertainties arising from this
217 approach, the threshold values for wind speed and precipitation were also increased as the track diameter increased
218 (**Table A1**). For a narrow storm track it is reasonable to assume that there would be damage shown in all pixels except
219 those where wind speed or precipitation did not exceed a relatively low threshold value. For wide storm tracks the
220 opposite applies; it is reasonable to assume that few of the pixels would show damage except where wind speed or
221 precipitation exceeded relatively high threshold values.

222

223 Data sources for the geolocation and diameter of an individual cyclone are described in detail in ‘Cyclone track and
224 diameter’. Wind speed and precipitation data were extracted from the ERA5-Land reanalysis data for land (ECMWF,
225 2019). The ERA5-Land reanalysis dataset has a spatial resolution of 9 km x 9 km and a time step of 1 hour. It is the
226 product of a data assimilation study conducted with the H-TESEL scheme by ERA5 IFS Cy45r1 and nudged by
227 climatological observations (ECMWF, 2018). The Cy45r1 reanalysis dataset shows statistically neutral results for the
228 position error of individual cyclones (ECMWF Confluence Wiki: Implementation of IFS cycle 45r1). The spatial
229 representation of the reanalysis data is reported to compare favorably with observational data (Chen et al., 2021)
230 outside the domain of this study. No reports on similar tests for the current study domain, i.e., East Asia, were found.
231 Furthermore, land cover maps released through the European Space Agency’s (ESA’s) Climate Change Initiative
232 (ESA, 2017) were used to restrict the analysis to forests. The CCI maps integrate observations from several space-
233 borne sensors, including MERIS, SPOT-VGT, AVHRR, and PROBA-V, into a continuous map with a 300 m
234 resolution from 1994 onwards.

235

236 Wind speed and precipitation data were spatially disaggregated and temporally aggregated to match the spatial and
237 temporal resolution of the ESA leaf area index (LAI) product (see below). Maximum wind speed and accumulative
238 precipitation were aggregated over time steps to match the 10-day resolution of the ESA LAI product. We preserved
239 the temporal resolution of the land cover map but aggregated the spatial resolution from 300 m to 1 km to match the
240 resolution of the ESA LAI product. During aggregation, the majority of land cover at the 300 m resolution was
241 assigned to the 1 km pixel resolution.

242

243 The oceanic Nino index (ONI) was retrieved from NOAA (NINO SST INDICES (NINO 1+2, 3, 3.4, 4; ONI AND
244 TNI), 2019). The oceanic Nino index was calculated and defined by comparing the 3-month running mean sea surface
245 temperature over the region from 5 degrees north to 5 degrees south and from 170 degrees west to 120 degrees west



246 with the 30 year climatology of sea surface temperature over the same region (Trenberth andStepaniak, 2001; The
247 climate data guide: Nino SST indices (Nino 1+2, 3, 3.4, 4; ONI and TNI)). A monthly seasonal oceanic Nino index
248 was used in this study. According to this method, El Nino events are characterized by an oceanic Nino index exceeding
249 0.5 K and La Nina events by an oceanic Nino index below -0.5 K. These thresholds relate to a warmer or a cooler
250 ocean state in the central tropical Pacific.

251

252 **Impact on leaf area of an individual cyclone**

253 Version 2 of ESA’s Climate Change Initiative product was used to calculate leaf area (LAI) in this study. The product
254 has a 1 km spatial resolution, a 10-day temporal resolution, and is available from 1999 onwards. The default LAI
255 product is distributed as a composite image using at least six valid observations on a pixel within a 30-day moving
256 window (Vergier et al., 2014). The composite image is drawn from satellite-based observations of the surface
257 reflectance in the red, near-infrared, and shortwave infrared from SPOT-VGT (from 1999 to May 2014) and PROBA-
258 V (from June 2014 to present). Gaps in missing observations are filled by the application of a relationship between
259 local weather and LAI dynamics. Gap filling resulted in errors on the LAI estimates of less than 0.18 (ref. (Martins et
260 al., 2020)). The spatiotemporal resolution of the LAI products was the coarsest of all data products used and therefore
261 determined the spatiotemporal resolution of the analysis as a whole. Moreover, the availability of the LAI product
262 determined the starting date for the study.

263

264 The impact of cyclones on leaf area was calculated by comparing the change in leaf area before and after the cyclone
265 in the affected area with changes before and after the cyclone in the reference area for each individual cyclone. In this
266 approach, the reference area serves as the control for the affected area, given that reference area and the affected area
267 may have a different size, the adjusted Hedge’s effect size (Rustad et al., 2001) can be used to calculate the effect size
268 of an individual cyclone on leaf area (**Eq. 1**). Using a reference area that is specific to each cyclone’s seasonal
269 dynamics, such as leaf phenology, is accounted for in the effect size. Effect size is thus a unitless quantifier which
270 describes the mean change in state, obtained by normalizing the mean difference in leaf area with the standard
271 deviation (**Eq. 1**). A positive or negative *ES* value indicates, respectively, an increase or decrease in leaf area following
272 the passage of a cyclone:

273

$$274 \quad ES = \frac{(\overline{LAI}_{bef} - \overline{LAI}_{aft})_{aff} - (\overline{LAI}_{bef} - \overline{LAI}_{aft})_{ref}}{\sigma}, \quad [1]$$

275

276 where *ES* is the event-based effect size for leaf area. The upper bar represents the mean of LAI in either the reference
277 (*ref*) or the affected (*aff*) area. The subscripts *ref* and *aff* denote the observation dates before and after the cyclone; σ
278 denotes the standard deviation of all observations within the storm track. Given the 10-day frequency of the ESA LAI
279 product, two LAI maps are used for the calculation of the *ES*, one to characterize the LAI 1 to 10 days before the
280 cyclone and the other to characterize the LAI 60 to 70 days after the cyclone. To distinguish between the affected and



281 reference areas the effect sizes were calculated for each event using the nine definitions. After applying the quality
282 control criteria (see below) a different number of events was available for each definition (**Table A1**).

283

284 The 60-day time frame was a compromise to avoid excessive data gaps in the LAI product when using a composite
285 LAI product. Because the LAI product reports LAI values within a 60-day window, the analysis had to be refined so
286 that this 60-day window never included the cyclone. The offset between the cyclone and a LAI observation from the
287 composite ESA LAI product was calculated by subtracting the date of the cyclone from the last observation date of
288 the LAI composite data before the cyclone or first observation date of the LAI composite data after the cyclone. Pixels
289 with a negative offset indicated that the composite data were likely to include observations from both before and after
290 the cyclone and were therefore discarded in the calculations of the effect size.

291

292 Starting the analysis from the actual storm tracks, as was the case in this study, allows for an unbiased assessment of
293 the impact of cyclones on forests (Blanc and Strobl, 2016), in contrast to studies that attribute decreases in leaf area
294 or related satellite-based indices to different disturbance agents including cyclones (Ozdogan et al., 2014; Takao et al.,
295 2014; Honkavaara et al., 2013; Forzieri et al., 2020). By design, the latter approach is not capable of identifying neutral
296 or positive impacts of cyclones on leaf area.

297

298 **Quality control**

299 The calculation of the effect size relies on having a similar LAI between the area that will become the affected area
300 and the area that will become the reference area after the passage of a cyclone. If the difference in LAI between the
301 reference and the affected area was over -0.25 but less than 0.25, the effect size calculated for this event was included
302 in subsequent analyses. The 0.25 threshold was derived through error propagation by considering that “similar LAI”
303 implies that the difference in LAI between the reference and affected area should be zero before the event. The
304 uncertainty from gap-filling satellite-based LAI products, i.e., 0.18 (ref. (Martins et al., 2020)) was used to derive a
305 reasonable threshold. Given that each LAI measurement may come with an uncertainty of 0.18 the difference between
306 two such measurements comes with an uncertainty of $0.25 (\sqrt{0.18^2 + 0.18^2})$.

307

308 The uncertainty of ES calculation through error propagation in equation (**Eq. 1**) is:

309

$$310 \quad \delta ES = |ES| * \sqrt{\left(\frac{\delta X}{X}\right)^2 + \left(\frac{\delta Y}{Y}\right)^2}, \quad [2]$$

311

312 where X is the nominator and Y is the denominator of **Eq. 1**. Given that each LAI observation is assumed to have an
313 uncertainty of 0.18, δX is constant at 0.36. The δY can be calculated by $\sqrt{n * (0.18)^2}/n$, where n is the number of
314 available observations. For each event, the quality of the ES calculation was examined by comparing the actual ES to



315 its uncertainty δES . Events for which $ES < \delta ES$ were not further analyzed. Events with an effect sizes between -0.18
316 and 0.18 were classified as neutral.

317

318 **Multivariate analysis**

319 Each tropical cyclone was characterized by its: (1) latitude of landfall (degrees); (2) intensity of the tropical cyclone
320 ($m\ s^{-1}$); (3) month of landfall; (4) maximum wind speed during passage over land ($m\ s^{-1}$); (5) accumulated rainfall
321 during passage over land (mm); (6) accumulated rainfall on land 30 days prior to landfall of the cyclone (mm); (7)
322 affected area during passage over land (Mha); (8) leaf area 30 days prior to landfall ($m^2\ m^{-2}$); (9) Standardized
323 Precipitation Evapotranspiration Index (SPEI) ($mm\ mm^{-1}$) as a drought proxy; and (10) oceanic Nino index the month
324 of landfall (K).

325

326 Characteristics 1 to 4 were retrieved from the JTWC database as detailed in ‘Cyclone track and track diameter’.
327 Characteristics 5 to 6 were retrieved from the ERA5-Land reanalysis data for land (ECMWF, 2019) and characteristic
328 7 from the analysis combining cyclone track, cyclone diameter and ERA5-Land reanalysis, as explained in ‘Area
329 affected by individual cyclones’. Characteristic 8 was taken from the LAI analysis as explained in ‘Impact on leaf area
330 of an individual cyclone’. For characteristic 9, Standardized Precipitation Evapotranspiration Index with a half-degree
331 by half-degree spatial resolution and a 10-day temporal resolution was used and combined with the cyclone masks
332 created in ‘Area affected by the individual cyclone’. Characteristic 10, the oceanic Nino index, was retrieved from
333 NOAA (NINO SST INDICES (NINO 1+2, 3, 3.4, 4; ONI AND TNI), 2019).

334

335 The characteristics were separated into two groups describing the condition of the land and ocean prior to the event
336 (“prior conditions” or PC group) and the characteristics of the tropical cyclone itself (“tropical cyclone characteristic”
337 or TCC group). The prior conditions group contained: pre-event LAI, pre-event drought state, pre-event accumulative
338 rainfall, oceanic Nino index, and month. Characteristics such as maximum wind speed, accumulative rainfall, cyclone
339 intensity, affected area, and latitude were used to describe the cyclone itself.

340

341 Factor analysis (Revelle, 2017) was used to reveal the collinearity among the selected variables in the “prior conditions”
342 and “tropical cyclone characteristic” group (**Table A2**). Collinearity was used to create 12 sets of mostly independent
343 characteristics (**Table A3**) which were used as the input for a random forest tree to identify the characteristics that
344 best explained the effect size for LAI. The random forest analysis was repeated for each of the 12 sets, but limited to
345 four-layer random forest trees, to identify the importance of the environmental variables on the tropical cyclone effect
346 size (not shown). Finally, to reduce the collinearity of the input variables, only the six variables with the highest
347 explanatory power were used to create a single decision tree which is shown in **Fig. 3**. For this, the recursive
348 partitioning approach was used with a maximum of five levels and a minimum of 20 samples in each node provided
349 by the R-rpart package (Therneau et al., 2019).

350



351 **Drought analysis**

352 The Standardized Precipitation Evapotranspiration Index (SPEI), is a proxy index for drought that represents the
353 climatic water balance and was used to assess the drought of a forest soil before and after the passage of an individual
354 tropical cyclone. The Standardized Precipitation Evapotranspiration Index data used in this study were retrieved from
355 the Global SPEI database (SPEIbase v2.6 (Beguería et al., 2014)), which is based on the CRU TS v.4.03 dataset (Harris
356 et al., 2020). In this study, the temporal resolution of the data was preserved but the spatial resolution was regrided
357 from the original half-degree to 1 km to match the resolution of the ESA LAI product. The contribution of an individual
358 tropical cyclone to ending a drought was evaluated by comparing the SPEI from affected and reference areas through
359 the following equation:

360

$$361 \delta SPEI = (SPEI_{imon})_{aff} - (SPEI_{imon})_{ref}, \quad [3]$$

362

363 where $\delta SPEI$ is the event-based change in drought. A positive or negative $\delta SPEI$ respectively denotes an increase or
364 decrease in available water resources following the passage of a tropical cyclone. The subscription *imon* represents
365 the integration time of available water resources in the calculation of the SPEI either in the reference (*ref*) or the
366 affected (*aff*) area which are defined in previous section. The same time window, i.e., 60-days, was applied for the
367 calculation of $\delta SPEI$ and event-based effect size for LAI.

368

369 **Acknowledgments**

370 Y.Y.C. would like to thank the National Center for High-performance Computing (NCHC) for sharing its
371 computational resources and data storage facilities. Y.Y.C. was funded through the Ministry of Science and
372 Technology (grant MOST 109-2111-M-001-011 and grant MOST 110-2111-M-001 -011).

373

374 **Data availability**

375 R-Scripts and all input data to performing the analysis and creating the plots can be found in the following web-based
376 repository <https://doi.org/10.5281/zenodo.6459795>. The database of event-based effect sizes, surface properties and
377 cyclone properties for each of the 1309 events (i.e., 145 \pm 42 unique tropical cyclones analyzed for nine related
378 definitions) can be accessed at:

379 <https://myspace.sinica.edu.tw/public.php?service=files&t=e2vJFnIASIdGgtvnfcqXAa51->

380 <aTChcjUgAJXk2mHjoZ1thVek8W9yeJx13GeHb>

381

382 **Author Contributions**

383 Y.Y.C. and S.L. designed the study. Y.Y.C. investigated and visualized the results. Y.Y.C. and S.L. contributed to the
384 interpretation of the results. S.L. wrote the original draft. S.L. and Y.Y.C. reviewed and edited the manuscript.

385

386 **Competing Interest Statement:** The authors declare no competing interests.



387 **References**

- 388 Altman, J., Ukhvatkina, O. N., Omelko, A. M., Macek, M., Plener, T., Pejcha, V., Cerny, T., Petrik, P., Srutek, M.,
389 Song, J.-S., Zhmerenetsky, A. A., Vozmishcheva, A. S., Krestov, P.V., Petrenko, T. Y., Treydte, K., and Dolezal, J.:
390 Poleward migration of the destructive effects of tropical cyclones during the 20th century, *Proc. Natl. Acad. Sci.*, 115,
391 11543–11548, <https://doi.org/10.1073/pnas.1808979115>, 2018.
- 392 Barbier, E. B.: Economic aspects of tropical deforestation in Southeast Asia, *Glob. Ecol. Biogeogr. Lett.*, 3, 215,
393 <https://doi.org/10.2307/2997771>, 1993.
- 394 Beguería, S., Vicente-Serrano, S. M., Reig, F., and Latorre, B.: Standardized precipitation evapotranspiration index
395 (SPEI) revisited: Parameter fitting, evapotranspiration models, tools, datasets and drought monitoring, *Int. J. Climatol.*,
396 34, 3001–3023, <https://doi.org/10.1002/joc.3887>, 2014.
- 397 Blanc, E. and Strobl, E.: Assessing the impact of typhoons on rice production in the Philippines, *J. Appl. Meteorol.*
398 *Climatol.*, 55, 993–1007, <https://doi.org/10.1175/jamc-d-15-0214.1>, 2016.
- 399 Bowen, T.: Social Protection in the Philippines “Emergency cash transfer” program in the Philippines, 1–16, 2016.
- 400 Bushnell, J. M., Cherrett, R. C., and Falvey, R. J.: Annual Tropical Cyclone Report 2018, 147pp., 2018.
- 401 Castañeda-Moya, E., Rivera-Monroy, V. H., Chambers, R. M., Zhao, X., Lamb-Wotton, L., Gorsky, A., Gaiser, E. E.,
402 Troxler, T. G., Kominoski, J. S., and Hiatt, M.: Hurricanes fertilize mangrove forests in the Gulf of Mexico (Florida
403 Everglades, USA), *Proc. Natl. Acad. Sci. U. S. A.*, 117, 4831–4841, <https://doi.org/10.1073/pnas.1908597117>, 2020.
- 404 Chambers, J. Q., Fisher, J. I., Zeng, H., Chapman, E. L., Baker, D. B., and Hurtt, G. C.: Hurricane Katrina’s carbon
405 footprint on U.S. Gulf coast forests, *Science*, 318, 1107–1107, <https://doi.org/10.1126/science.1148913>, 2007.
- 406 Chang, C.-T., Lee Shaner, P.-J., Wang, H.-H., and Lin, T.-C.: Resilience of a subtropical rainforest to annual typhoon
407 disturbance: Lessons from 25-year data of leaf area index, *For. Ecol. Manage.*, 470–471, 118210,
408 <https://doi.org/10.1016/j.foreco.2020.118210>, 2020a.
- 409 Chang, C.-T., Shih, Y. T., Lee, L. C., Lee, J. Y., Lee, T. Y., Lin, T. C., and Huang, J. C.: Effects of land cover and
410 atmospheric input on nutrient budget in subtropical mountainous rivers, northeastern taiwan, 12,
411 <https://doi.org/10.3390/w12102800>, 2020b.
- 412 Chen, Y.-Y., Gardiner, B., Pasztor, F., Blennow, K., Ryder, J., Valade, A., Naudts, K., Otto, J., McGrath, M. J.,
413 Planque, C., and Luyssaert, S.: Simulating damage for wind storms in the land surface model ORCHIDEE-CAN
414 (revision 4262), *Geosci. Model Dev.*, 11, 771–791, <https://doi.org/10.5194/gmd-11-771-2018>, 2018.
- 415 Chen, Y., Sharma, S., Zhou, X., Yang, K., Li, X., Niu, X., Hu, X., and Khadka, N.: Spatial performance of multiple
416 reanalysis precipitation datasets on the southern slope of central Himalaya, *Atmos. Res.*, 250, 105365,
417 <https://doi.org/10.1016/j.atmosres.2020.105365>, 2021.
- 418 Chiu, C.-M., Chien, C.-T., Nigh, G., and Chung, C.-H.: Influence of climate on tree mortality in Taiwan (Taiwania
419 *cryptomerioides*) stands in Taiwan, *New Zeal. J. For. Sci.*, 48, <https://doi.org/10.1186/A40490-018-0111-0>, 2018.
- 420 Choi, K.-S., Wu, C.-C., and Cha, E.-J.: Change of tropical cyclone activity by Pacific-Japan teleconnection pattern in
421 the western North Pacific, *J. Geophys. Res. Atmos.*, 115, 1–13, <https://doi.org/10.1029/2010JD013866>, 2010.



- 422 Choi, K.-S., Kim, D.-W., and Byun, H.-R.: Relationship between summer drought of mid-latitudes in East Asia and
423 tropical cyclone genesis frequency in the Western North Pacific, in: *Advances in Geosciences (A 6-Volume Set)*,
424 edited by: Satake, K. and Wu, C.-C., World Scientific Publishing Co. Pte. Ltd., 1–13,
425 https://doi.org/10.1142/9789814355315_0001, 2011.
- 426 Chou, C., Huang, L.-F., Tseng, L., Tu, J.-Y., and Tan, P.-H.: Annual cycle of rainfall in the Western North Pacific
427 and East Asian sector, *J. Clim.*, 22, 2073–2094, <https://doi.org/10.1175/2008JCLI2538.1>, 2009.
- 428 The Joint Typhoon Warning Center Tropical Cyclone Best-Tracks, 1945-2000:
429 <https://www.metoc.navy.mil/jtwc/products/best-tracks/tc-bt-report.html>, last access: 25June2019.
- 430 Curran, T. J., Brown, R. L., Edwards, E., Hopkins, K., Kelley, C., McCarthy, E., Pounds, E., Solan, R., and Wolf, J.:
431 Plant functional traits explain interspecific differences in immediate cyclone damage to trees of an endangered
432 rainforest community in north Queensland, *Austral Ecol.*, 33, 451–461, <https://doi.org/10.1111/j.1442->
433 [9993.2008.01900.x](https://doi.org/10.1111/j.1442-9993.2008.01900.x), 2008.
- 434 Douglas, I.: Hydrological investigations of forest disturbance and land cover impacts in South–East Asia: a review,
435 *Philos. Trans. R. Soc. London. Ser. B Biol. Sci.*, 354, 1725–1738, <https://doi.org/10.1098/rstb.1999.0516>, 1999.
- 436 Dvorak, V. F.: Tropical cyclone intensity analysis using satellite data,
437 <https://repository.library.noaa.gov/view/noaa/19322>, 1984.
- 438 Dvorak, V. F., Smigielski, F. J., and States., U.: A workbook on tropical clouds and cloud systems observed in satellite
439 imagery, file://catalog.hathitrust.org/Record/002715963, 1990.
- 440 ECMWF: IFS Documentation CY45R1 - Part II: Data assimilation, in: IFS Documentation CY45R1, ECMWF,
441 <https://doi.org/10.21957/a3ri44ig4>, 2018.
- 442 ECMWF: ERA5-Land hourly data from 1981 to present, <https://doi.org/10.24381/cds.e2161bac>, 2019.
- 443 Eloy, C., Fournier, M., Lacoite, A., and Moulia, B.: Wind loads and competition for light sculpt trees into self-similar
444 structures, *Nat. Commun.*, 8, 1–11, <https://doi.org/10.1038/A41467-017-00995-6>, 2017.
- 445 ESA: Land Cover CCI Product User Guide Version 2, 105pp., 2017.
- 446 Forzieri, G., Pecchi, M., Girardello, M., Mauri, A., Klaus, M., Nikolov, C., Rüetschi, M., Gardiner, B., Tomaščík, J.,
447 Small, D., Nistor, C., Jonikavicius, D., Spinoni, J., Feyen, L., Giannetti, F., Comino, R., Wolynski, A., Pirotti, F.,
448 Maistrelli, F., Savulescu, I., Wurpillot-Lucas, S., Karlsson, S., Zieba-Kulawik, K., Strejczek-Jazwinska, P., Mokroš,
449 M., Franz, S., Krejci, L., Haidu, I., Nilsson, M., Wezyk, P., Catani, F., Chen, Y.-Y., Luyssaert, S., Chirici, G.,
450 Cescatti, A., and Beck, P. S. A.: A spatially explicit database of wind disturbances in European forests over the
451 period 2000–2018, *Earth Syst. Sci. Data*, 12, 257–276, <https://doi.org/10.5194/essd-12-257-2020>, 2020.
- 452 Harris, I., Osborn, T. J., Jones, P., and Lister, D.: Version 4 of the CRU TS monthly high-resolution gridded
453 multivariate climate dataset, *Sci. Data*, 7, 1–18, <https://doi.org/10.1038/A41597-020-0453-3>, 2020.
- 454 Honkavaara, E., Litkey, P., and Nurminen, K.: Automatic storm damage detection in forests using high-altitude
455 photogrammetric imagery, *Remote Sens.*, 5, 1405–1424, <https://doi.org/10.3390/rs5031405>, 2013.
- 456 Kaplan, J. and Demaria, M.: On the decay of tropical cyclone winds after landfall in the New England Area, *J. Appl.*
457 *Meteorol.*, 40, 280–286, [https://doi.org/10.1175/1520-0450\(2001\)040<0280:OTDOTC>2.0.CO;2](https://doi.org/10.1175/1520-0450(2001)040<0280:OTDOTC>2.0.CO;2), 2001.



- 458 Kubota, H., Kosaka, Y., and Xie, S. P.: A 117-year long index of the Pacific-Japan pattern with application to
459 interdecadal variability, *Int. J. Climatol.*, 36, 1575–1589, <https://doi.org/10.1002/joc.4441>, 2016.
- 460 Landsea, C. W.: Climate variability of tropical cyclones: Past, Present and Future, in: *Storms*, edited by: Pielke, R. A.
461 S. and Pielke, R. A. J., Routledge, New York, 220–241, 2000.
- 462 Lin, T.-C., Hamburg, S., Lin, K.-C., Wang, L.-J., Chang, C.-T., Hsia, Y.-J., Vadeboncoeur, M. A., Mabry McMullen,
463 C. M., and Liu, C.-P.: Typhoon disturbance and forest dynamics: Lessons from a Northwest Pacific subtropical forest,
464 14, 127–143, <https://doi.org/10.1007/s10021-010-9399-1>, 2011.
- 465 Lin, T. C., Hogan, J. A., and Chang, C. Te: Tropical Cyclone Ecology: A Scale-Link Perspective, *Trends Ecol. Evol.*,
466 35, 594–604, <https://doi.org/10.1016/j.tree.2020.02.012>, 2020.
- 467 Louf, J. F., Nelson, L., Kang, H., Song, P. N., Zehnbauer, T., and Jung, S.: How wind drives the correlation between
468 leaf shape and mechanical properties, *Sci. Rep.*, 8, 1–7, <https://doi.org/10.1038/A41598-018-34588-0>, 2018.
- 469 Lu, Y., Yu, H., Yang, Q., Xu, M., Zheng, F., and Zhu, J.: Post-Disaster Survey of Typhoon Megi in Wenzhou City,
470 *Trop. Cyclone Res. Rev.*, 6, 34–39, <https://doi.org/10.6057/2017TCRRh1.04>, 2017.
- 471 ECMWF Confluence Wiki: Implementation of IFS cycle 45r1:
472 <https://confluence.ecmwf.int/display/FCST/Implementation+of+IFS+cycle+45r1#ImplementationofIFScycle45r1>-
473 Tropicalcyclones.
- 474 Mabry, C. M., Hamburg, S. P., Lin, T.-C., Horng, F. W., King, H. B., and Hsia, Y. J.: Typhoon disturbance and stand-
475 level damage patterns at a subtropical forest in Taiwan, *Biotropica*, 30, 238–250, <https://doi.org/10.1111/j.1744->
476 [7429.1998.tb00058.x](https://doi.org/10.1111/j.1744-7429.1998.tb00058.x), 1998.
- 477 Martins, J. P., Trigo, I., and Freitas, S. C. de: Copernicus Global Land Operations ”Vegetation and Energy” “CGLOPS-
478 1,” *Copernicus Glob. L. Oper.*, 1–93, 2020.
- 479 McDowell, N. G., Allen, C. D., Anderson-Teixeira, K., Aukema, B. H., Bond-Lamberty, B., Chini, L., Clark, J. S.,
480 Dietze, M., Grossiord, C., Hanbury-Brown, A., Hurtt, G. C., Jackson, R. B., Johnson, D. J., Kueppers, L., Lichstein,
481 J. W., Ogle, K., Poulter, B., Pugh, T. A. M., Seidl, R., Turner, M. G., Uriarte, M., Walker, A. P., and Xu, C.: Pervasive
482 shifts in forest dynamics in a changing world, *Science (80-)*, 368, <https://doi.org/10.1126/science.aaz9463>, 2020.
- 483 Mei, W. and Xie, S. P.: Intensification of landfalling typhoons over the northwest Pacific since the late 1970s, *Nat.*
484 *Geosci.*, 9, 753–757, <https://doi.org/10.1038/ngeo2792>, 2016.
- 485 NINO SST INDICES (NINO 1+2, 3, 3.4, 4; ONI AND TNI): [https://climatedataguide.ucar.edu/climate-data/nino-sst-](https://climatedataguide.ucar.edu/climate-data/nino-sst-indices-nino-12-3-34-4-oni-and-tni)
486 [indices-nino-12-3-34-4-oni-and-tni](https://climatedataguide.ucar.edu/climate-data/nino-sst-indices-nino-12-3-34-4-oni-and-tni), last access: 28February2019.
- 487 Negrón-Juárez, R. I., Chambers, J. Q., Guimaraes, G., Zeng, H., Raupp, C. F. M., Marra, D. M., Ribeiro, G. H. P. M.,
488 Saatchi, S. S., Nelson, B. W., and Higuchi, N.: Widespread Amazon forest tree mortality from a single cross-basin
489 squall line event, *Geophys. Res. Lett.*, 37, 1–5, <https://doi.org/10.1029/2010GL043733>, 2010.
- 490 Nelson, B. W., Kapos, V., Adams, J. B., Oliveira, W. J., Braun, O. P. G., and doAmaral, I. L.: Forest disturbance by
491 large blowdowns in the Brazilian Amazon, *Ecology*, 75, 853–858, <https://doi.org/10.2307/1941742>, 1994.
- 492 OCHA: Infrastructure Federation of Red Cross and Red Crescent Societies, Philippines : Typhoon Megi, 1–7pp., 2010.



- 493 Ozdogan, M., Vladimirova, N., Radeloff, V. C., Krylov, A., Wolter, P. T., and Baumann, M.: Landsat remote sensing
494 of forest windfall disturbance, *Remote Sens. Environ.*, 143, 171–179, <https://doi.org/10.1016/j.rse.2013.12.020>, 2014.
- 495 Revelle, R. W.: psych; <https://cran.r-project.org/package=psych>, 2017.
- 496 Rustad, L. E., Campbell, J. L., Marion, G. M., Norby, R. J., Mitchell, M. J., Hartley, A. E., Cornelissen, J. H. C.,
497 Gurevitch, J., Alward, R., Beier, C., Burke, I., Canadell, J., Callaghan, T., Christensen, T. R., Fahnestock, J.,
498 Fernandez, I., Harte, J., Hollister, R., John, H., Ineson, P., Johnson, M. G., Jonasson, S., John, L., Linder, S., Lukewille,
499 A., Masters, G., Melillo, J., Mickelsen, A., Neill, C., Olszyk, D. M., Press, M., Pregitzer, K., Robinson, C., Rygiewiez,
500 P. T., Sala, O., Schmidt, I. K., Shaver, G., Thompson, K., Tingey, D. T., Verburg, P., Wall, D., Welker, J., and Wright,
501 R.: A meta-analysis of the response of soil respiration, net nitrogen mineralization, and aboveground plant growth to
502 experimental ecosystem warming, *Oecologia*, 126, 543–562, <https://doi.org/10.1007/s004420000544>, 2001.
- 503 Stuijvenolt Allen, J., Simon Wang, S. -Y., LaPlante, M. D., and Yoon, J.: Three Western Pacific Typhoons
504 Strengthened Fire Weather in the Recent Northwest U.S. Conflagration, *Geophys. Res. Lett.*, 48,
505 <https://doi.org/10.1029/2020GL091430>, 2021.
- 506 Takao, G., Saigusa, N., Yamagata, Y., Hayashi, M., and Oguma, H.: Quantitative assessment of the impact of typhoon
507 disturbance on a Japanese forest using satellite laser altimetry, *Remote Sens. Environ.*, 156, 216–225,
508 <https://doi.org/10.1016/j.rse.2014.09.028>, 2014.
- 509 Tang, S., Lin, T.-C., Hsia, Y.-J., Hamburg, S. P., and Lin, K.-C.: Typhoon effects on litterfall in a subtropical forest,
510 *Can. J. For. Res.*, 33, 2184–2192, <https://doi.org/10.1139/x03-154>, 2003.
- 511 Therneau, T., Atkinson, B., and Ripley, B.: rpart: Recursive partitioning for classification, regression and survival
512 trees., CRAN R package version 4.1-15, 2019.
- 513 The climate data guide: Nino SST indices (Nino 1+2, 3, 3.4, 4; ONI and TNI):
- 514 Trenberth, K. E. and Stepaniak, D. P.: Indices of El Niño evolution, *J. Clim.*, 14, 1697–1701,
515 [https://doi.org/10.1175/1520-0442\(2001\)014<1697:LIOENO>2.0.CO;2](https://doi.org/10.1175/1520-0442(2001)014<1697:LIOENO>2.0.CO;2), 2001.
- 516 Uriarte, M., Thompson, J., and Zimmerman, J. K.: Hurricane María tripled stem breaks and doubled tree mortality
517 relative to other major storms, *Nat. Commun.*, 10, 1–7, <https://doi.org/10.1038/A41467-019-09319-2>, 2019.
- 518 Verger, A., Baret, F., and Weiss, M.: Near real-time vegetation monitoring at global scale, *IEEE J. Sel. Top. Appl.*
519 *Earth Obs. Remote Sens.*, 7, 3473–3481, <https://doi.org/10.1109/JSTARS.2014.2328632>, 2014.
- 520 Vickers, B., Kant, P., Bleaney, A., Milne, S., Suzuki, R., Ramos, L. T., Pohnan, E., and Lasco, R. D.: Forests and
521 Climate Change Working Paper 7: Forests and Climate Change in the Asia-Pacific Region, Food and Agriculture
522 Organization of the United Nations, Rome, 1–126pp., 2010.
- 523 Virost, E., Ponomarenko, A., Dehandschoewercker, Quéré, D., and Clanet, C.: Critical wind speed at which trees break,
524 *Phys. Rev. E*, 93, <https://doi.org/10.1103/PhysRevE.93.023001>, 2016.
- 525 Wang, H.-C., Wang, S.-F., Lin, K.-C., Lee Shaner, P.-J., and Lin, T.-C.: Litterfall and Element Fluxes in a Natural
526 Hardwood Forest and a Chinese-fir Plantation Experiencing Frequent Typhoon Disturbance in Central Taiwan,
527 *Biotropica*, 45, 541–548, <https://doi.org/10.1111/btp.12048>, 2013.



528 Willoughby, H. E. and Rahn, M. E.: Parametric representation of the primary hurricane vortex. Part I: Observations
529 and evaluation of the Holland (1980) model, *Mon. Weather Rev.*, 132, 3033–3048,
530 <https://doi.org/10.1175/MWR2831.1>, 2004.

531 WMO: *Global Guide to Tropical Cyclone Forecasting*, 399pp., 2017.

532 Xi, W.: Synergistic effects of tropical cyclones on forest ecosystems: a global synthesis, *J. For. Res.*, 26,
533 <https://doi.org/10.1007/s11676-015-0018-z>, 2015.

534 Yang, H.-H., Chen, S.-Y. C., Chien, S.-Y., and Li, W.-S.: *Forensic Investigation of Typhoon Morakot Disaster:*
535 *Nansalu and Daniao Village Case Study (NCDR 102-T28)*, Taipei, 45pp., 2014.

536 Yoo, J., Kwon, H.-H. H., So, B.-J. J., Rajagopalan, B., and Kim, T.-W. W.: Identifying the role of typhoons as drought
537 busters in South Korea based on hidden Markov chain models, *Geophys. Res. Lett.*, 42, 2797–2804,
538 <https://doi.org/10.1002/2015GL063753>, 2015.

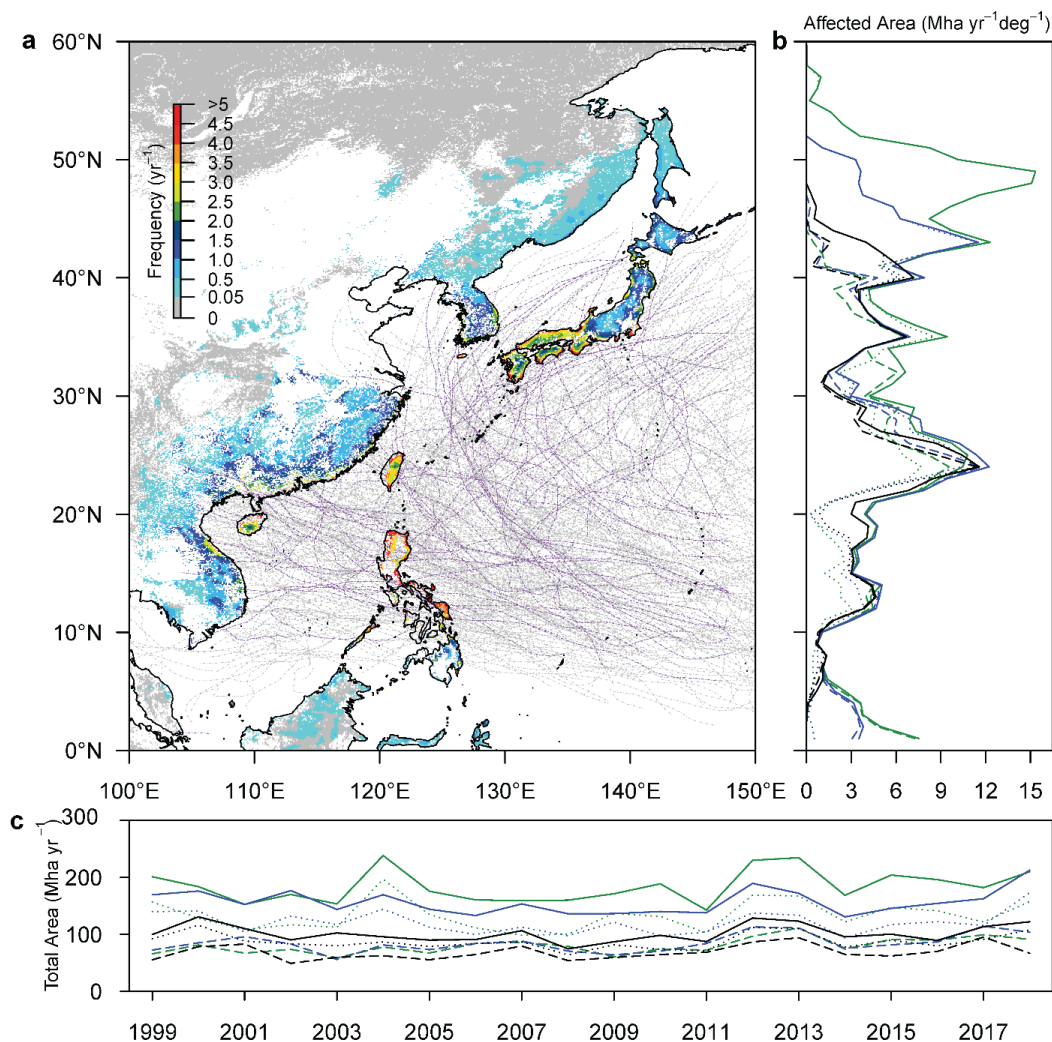
539 Zhao, T. and Dai, A.: Uncertainties in historical changes and future projections of drought. Part II: model-simulated
540 historical and future drought changes, *Clim. Change*, 144, 535–548, <https://doi.org/10.1007/s10584-016-1742-x>, 2017.

541

542



543 **Figures and Tables**

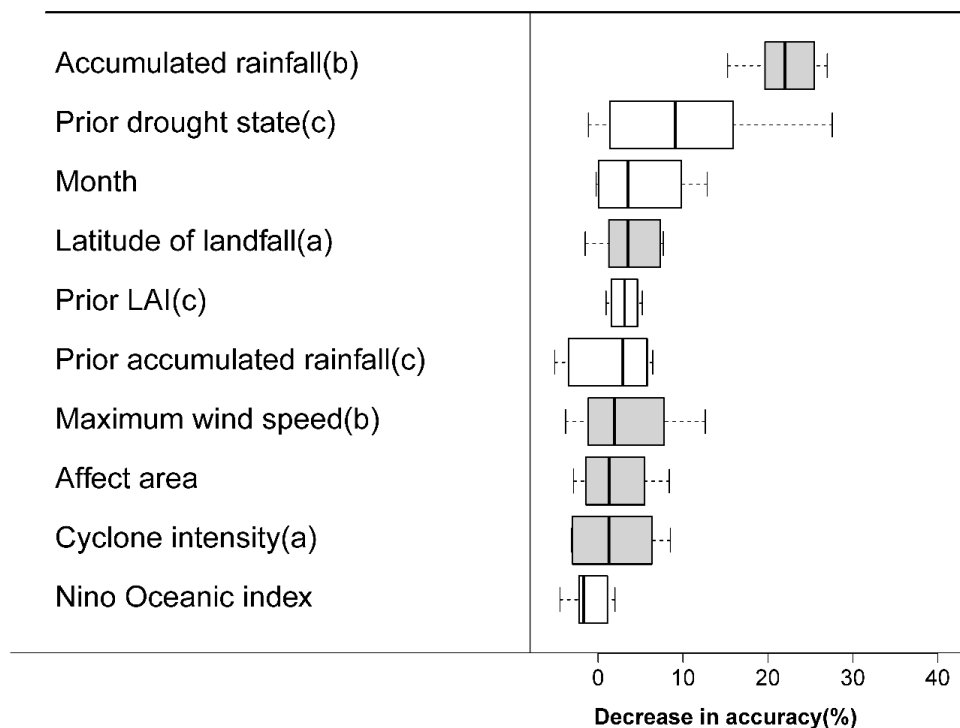


544

545 **Figure 1.** Spatial and temporal patterns of potential forest damage by tropical cyclones in East Asia. (A) Return
546 frequency (yr^{-1}) of tropical cyclones between 1999 and 2018. Pixels where forest is the main land cover are shaded.
547 The color of the shading represents the return frequency of tropical cyclones based on definition 3b for the affected
548 area (Table A1). The dot-dashed lines show the cyclone tracks between 1999 and 2018. The purple lines indicate the
549 cases passed the QC/QA criteria used in this study. (B) Temporal dynamics of the total potentially damaged forest
550 area (Mha yr^{-1}) for all nine definitions of affected area. (C) Latitudinal gradients of potentially damaged forest area
551 ($\text{Mha yr}^{-1} \text{ deg}^{-1}$) between 1999 to 2018 for all nine definitions of affected area. The dotted lines show the “wind



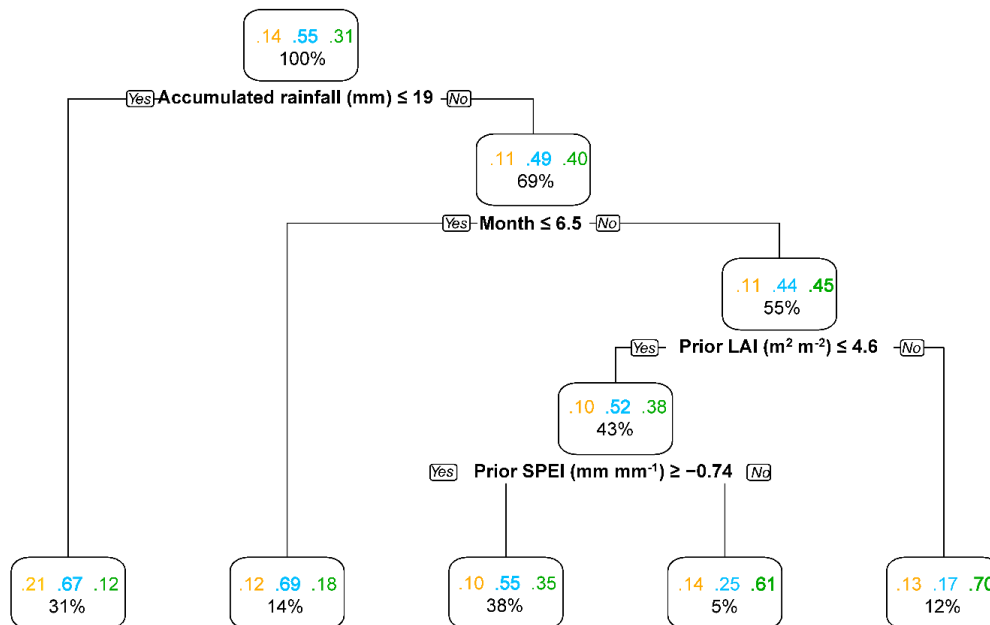
552 only” definitions (group 1), the dashed lines show the “rainfall only” definitions (group 2), and the solid lines show
553 the “combined” definitions (group 3). The black, blue and green colored lines represent definitions a, b and c,
554 respectively, within each group. Definitions are detailed in Table A1.
555



556

557 **Figure 2.** Importance of the five surface (white) and five cyclone (grey) characteristics in explaining the LAI response
558 to the passage of a tropical cyclone. The boxplots show the 95, 75, 50, 25 and 5 percentiles of the decrease in accuracy.
559 The letters a, b and c following the label of a characteristic indicate collinearity between the variables (Table A2).
560 Each boxplot contains the results of 12 random forest analyses fitted with different combinations of largely
561 uncorrelated characteristics (Table A3). Each random forest analysis is based on 1309 cases coming from the 145 ±
562 42 individual tropical cyclones for which the impact was quantified according to nine related definitions (Table A1).
563 The medians were used to sort the cyclone and surface characteristics according to decreasing importance.

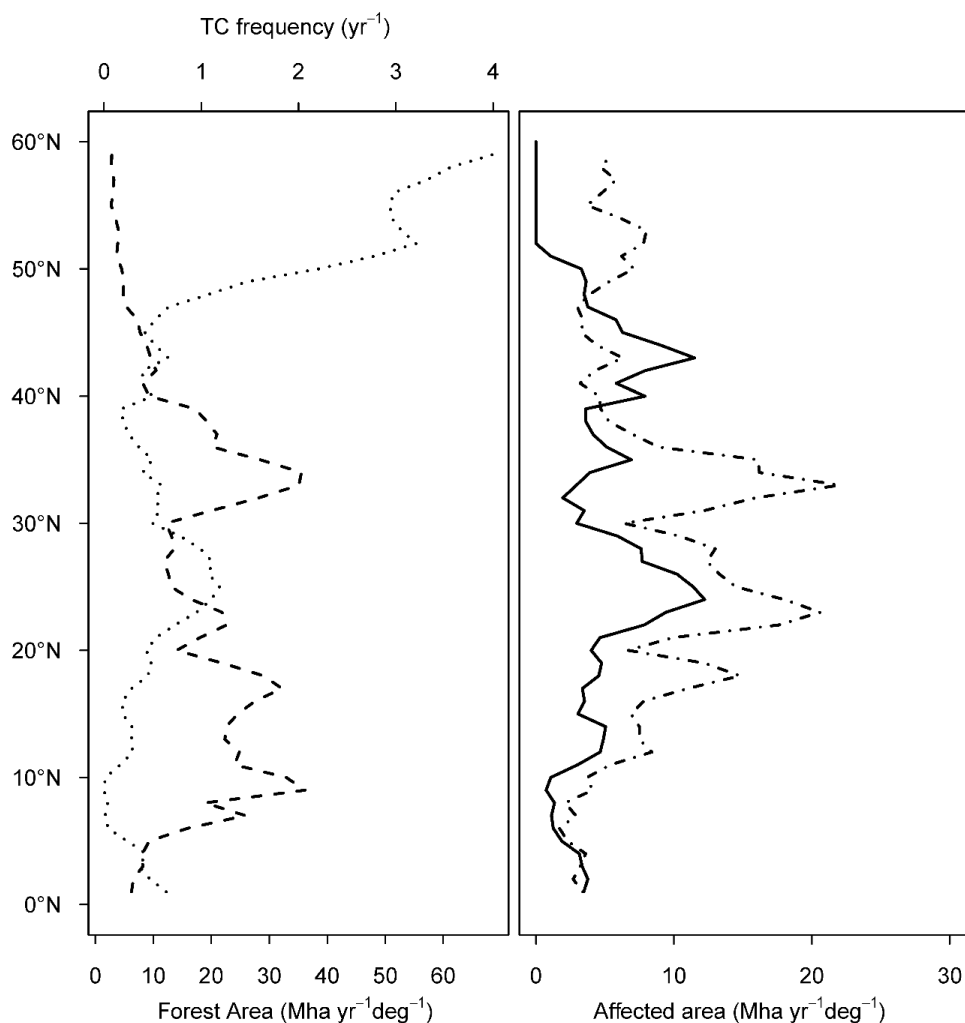
564



565
 566 **Figure 3.** Environmental drivers contributing to an increase of LAI following the passage of a tropical cyclone. The
 567 fractions of a negative, neutral and positive effect size are listed for each box in respectively orange, blue, and green.
 568 The number of events is listed as the percentage of the total number of events in the random tree (n=1309).
 569



570 **Appendix**

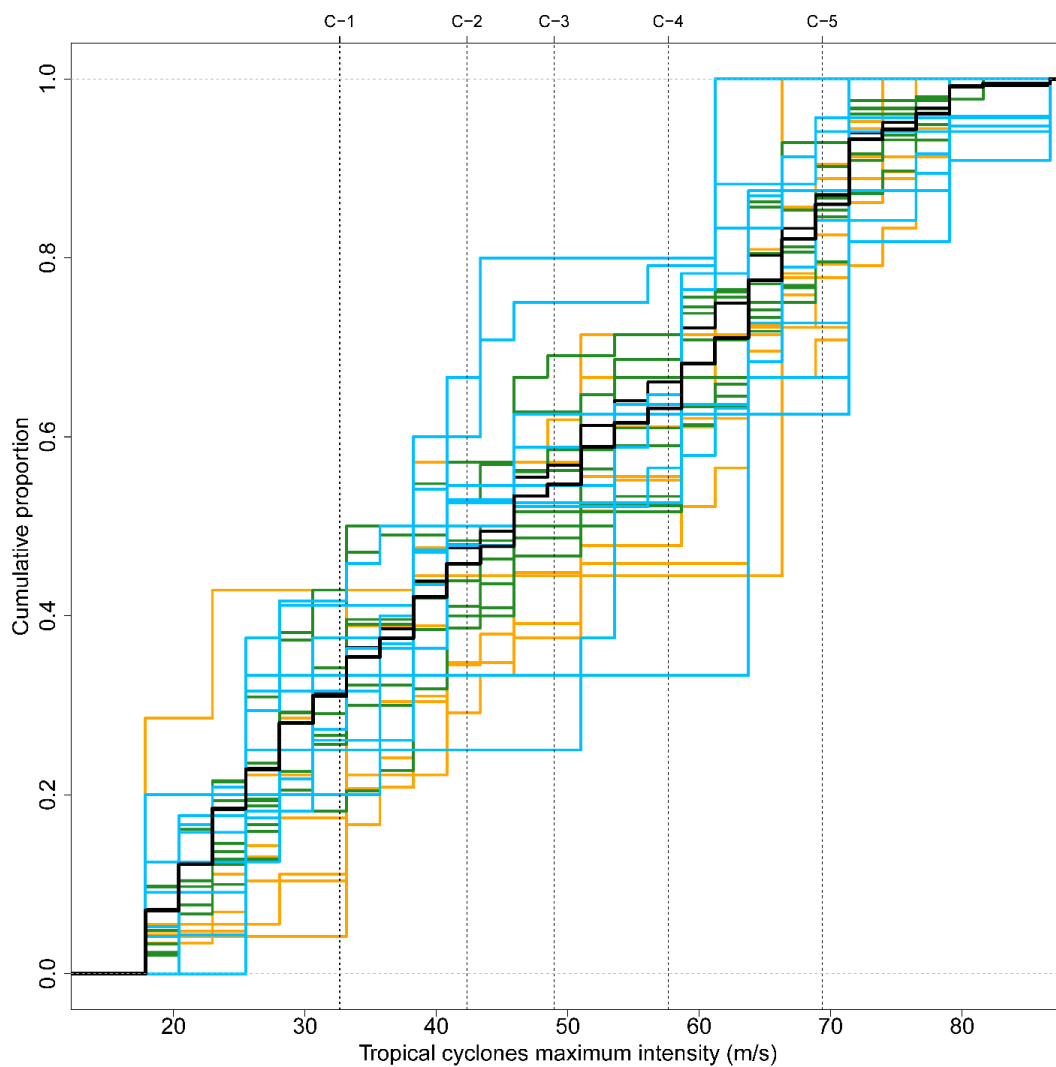


571

572 **Figure A1.** Contribution of return frequency and forest cover to the affected area: (A) zonal average of forest
573 coverage (dotted line; Mha deg^{-1}) and the return frequency (dashed line; yr^{-1}) of TC from 0 degrees N to 60 degrees
574 N averaged over Eastern Asia, as defined in this study; (B) Zonal average of the interaction between return
575 frequency and forest cover, calculated by multiplying the return frequency with the forest cover (dotdash line; Mha
576 $\text{yr}^{-1} \text{deg}^{-1}$) and the estimated zonal average of the annual affected forest area (full line; $\text{Mha yr}^{-1} \text{deg}^{-1}$) for definition
577 3b (Table A1). Correlations between return frequency and affected area (Pearson correlation coefficient = -0.35, p-
578 value < 0.01, n = 60), forest cover and affected area (Pearson correlation coefficient = 0.089, p-value = 0.5, n = 60)



579 and frequency x cover and affected area (Pearson correlation coefficient = 0.44, p-value < 0.01, n = 60). The latter
580 thus correlates best with the zonal variation in the affected area and was therefore shown in subplot B.
581

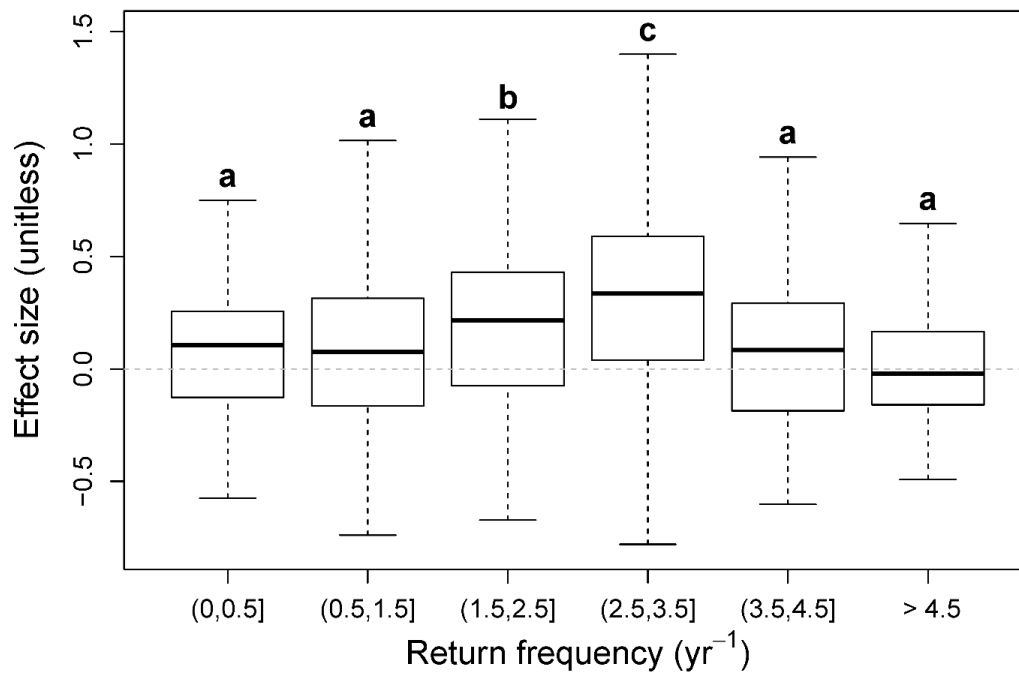


582

583 **Figure A2.** Cumulative distribution function of the tropical cyclones as a function of their maximum intensity. The
584 black solid line shows the distribution of the 580 events that occurred between 1999 to 2018. The grey lines show
585 the distributions obtained using all nine definitions to calculate the effect sizes: intensity distribution for tropical

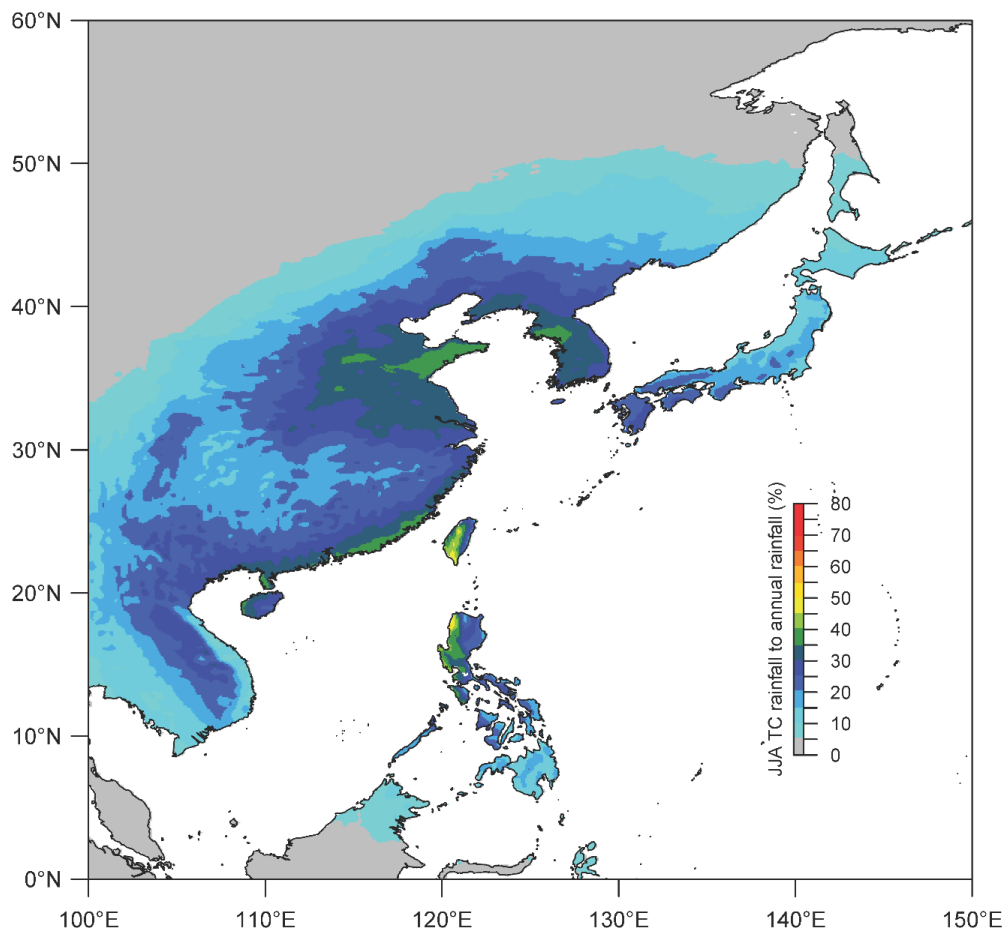


586 cyclones with a negative effect size (orange); intensity distribution for tropical cyclones with a neutral effect size
587 (blue); and intensity distribution for tropical cyclones with a positive effect size (green).
588



589

590 **Figure A3.** Box-wisher plots of the effect size on LAI 60 days following the passage of a tropical cyclone stratified
591 by the return frequency of the tropical cyclones for the location where the cyclone made landfall. The letters a, b and
592 c on top of the box whiskers show the different groups identified by a Tukey multiple comparison.



593

594 **Figure A4.** Share (%) of the rainfall contributed by tropical cyclones in June, July and August to the total annual
595 rainfall over Eastern Asia between 1999 to 2018.



596 **Table A1.** Criteria for distinguishing between the affected and reference areas following the passage of an individual
 597 cyclone and the number of events according to each specific definition. Group 1 groups definitions based on wind
 598 speed, group 2 definitions are based on precipitation and group 3 definitions are based on both wind speed and
 599 precipitation. All three definitions include an estimate of storm path based on a multiple of the reported storm diameter.
 600 Column A denotes the number of events for which data were lacking so that the effect size could not be calculated;
 601 column B denotes the number of events for which all required data were available; column C denotes the subset of B
 602 for which the data passed the quality control (see Quality Control); ES refers to effect size. A total of 580 unique
 603 tropical cyclones were considered in this study.

Group	Affected area	Reference area	A	B	C	Negative <i>ES</i>	Neutral <i>ES</i>	Positive <i>ES</i>
1.a	> 8 ms ⁻¹ and <2 diameters	< 8 ms ⁻¹ and <2 diameters	342	238	114	19	62	33
1.b	> 10 ms ⁻¹ and <3 diameters	< 10 ms ⁻¹ and <3 diameters	305	275	188	31	113	44
1.c	> 12 ms ⁻¹ and <4 diameters	< 12 ms ⁻¹ and <4 diameters	291	289	178	27	105	46
2.a	> 60 mm and <2 diameters	< 60 mm and <2 diameters	338	242	117	18	55	44
2.b	> 80 mm and <3 diameters	< 80 mm and <3 diameters	315	265	136	10	69	57
2.c	> 100 mm and <4 diameters	< 100 mm and <4 diameters	311	269	88	7	36	45
3.a	(> 8 ms ⁻¹ or > 60 mm) and <2 diameters	(< 8 ms ⁻¹ or < 60 mm) and < 2 diameters	352	228	105	21	50	34
3.b	(> 10 ms ⁻¹ or > 80 mm) and <3 diameters	(< 10 ms ⁻¹ or < 80 mm) and < 3 diameters	304	276	196	29	114	53
3.c	(> 12 ms ⁻¹ or > 100 mm) and <4 diameters	(< 12 ms ⁻¹ or < 100 mm) and < 4 diameters	288	292	187	27	110	50
Mean			316	264	145	21	79	45
Std			22	22	42	8	31	8
Mean (%)			54	46	25	14	55	31
Std (%)			4	4	7	6	21	6

604



605 **Table A2.** Loadings of each characteristic on three axes and collinearity between variables within the same group (See
 606 section “multivariate analysis” for more details). Collinearity was used to build random forests with largely
 607 uncorrelated explanatory variables (**Fig. 2 & 3**). Factor analysis was performed separately for each group. Given the
 608 exploratory nature of this analysis, a factor loading of 0.7 was used as a cut-off and those exceeding that level are
 609 highlighted in bold face. Here, TCC refers to characteristics describing the tropical cyclone itself and PC to the
 610 characteristics of the land and ocean prior to the cyclone.

Group	Characteristics	FC1	FC2	FC3	Collinearity
TCC	Maximum wind speed during passage over land (m s^{-1})	0.01	0.79	0.21	a
	Accumulated rainfall during passage over land (mm)	-0.18	-0.83	0.08	b
	Latitude of landfall (degrees)	0.83	0.04	0.13	c
	Intensity of the tropical cyclone, gusts (m s^{-1})	0.87	0.14	0.06	c
	Affected area during passage over land (ha)	0.15	0.09	0.97	d
PC	Month of landfall	-0.12	0.01	0.90	d
	Prior Accumulated rainfall (30 days prior to landfall (mm))	0.80	-0.25	0.02	e
	Prior LAI (30 days prior to landfall ($\text{m}^2 \text{m}^{-2}$))	0.82	0.23	-0.15	e
	Oceanic Nino index the month of landfall (K)	-0.02	0.96	0.08	f
	Prior drought state (SPEI, 30 days prior to landfall (mm mm^{-1}))	0.17	-0.71	0.32	g

611



612

613 **Table A3.** Sets of largely independent variables were used as input in the random forest analysis. Details of the
 614 variables are given in the section “multivariate analysis”. The justification for the groups is given by the collinearity
 615 as reported in Table S2. LAI stands for leaf area index and SPEI stands for Standardized Precipitation
 616 Evapotranspiration Index.

Set	Group with tropical cyclone characteristics (TCC)	Group with land characteristics prior to the cyclone (PC)
1	Maximum wind speed, affected area & latitude	pre-event LAI, oceanic Nino index & month
2	Accumulated rainfall, affected area & latitude	pre-event LAI, oceanic Nino index & month
3	Maximum wind speed, cyclone intensity & affected area	pre-event LAI, oceanic Nino index & month
4	Accumulated rainfall, cyclone intensity & affected area	pre-event LAI, oceanic Nino index & month
5	Maximum wind speed, affected area & latitude	pre-event SPEI, oceanic Nino index & month
6	Accumulated rainfall, affected area & latitude	pre-event SPEI, oceanic Nino index & month
7	Maximum wind speed, cyclone intensity & affected area	pre-event SPEI, oceanic Nino index & month
8	Accumulated rainfall, cyclone intensity & affected area	pre-event SPEI, oceanic Nino index & month
9	Maximum wind speed, affected area & latitude	pre-event accumulative rainfall, oceanic Nino index & month
10	Accumulated rainfall, affected area & latitude	pre-event accumulative rainfall, oceanic Nino index & month
11	Maximum wind speed, cyclone intensity & affected area	pre-event accumulative rainfall, oceanic Nino index & month
12	Accumulated rainfall, cyclone intensity & affected area	pre-event accumulative rainfall, oceanic Nino index & month